Zhu, B., Ren, G., Cryan, M. J., Gao, Y., Lian, Y., Li, H., ... Jian, S. (2015). Biomimetic 'moth-eye' anti-reflection boundary for graphene plasmons circuits. Journal of Optics, 17(12), [125012]. DOI: 10.1088/2040-8978/17/12/125012

Biomimetic 'moth-eye' anti-reflection design on the graphene sheet

Bofeng Zhu,[1,2,3] Guobin Ren,[1,2,*] Martin J. Cryan,[3] Yixiao Gao,[1,2] Yudong Lian,[1,2] Haisu Li,[1,2] Chenglong Wan,[3] and Shuisheng Jian[1,2]

[1]*Key Lab of All Optical Network & Advanced Telecommunication Network of EMC, Beijing Jiaotong University, Beijing 100044, China*

[2]*Institute of Lightwave Technology, Beijing Jiaotong University, Beijing 100044, China*

[3]*Department of Electrical and Electronic Engineering, University of Bristol, Bristol, UK*

gbren@bjtu.edu.cn.

Abstract: In this paper we propose the biomimetic moth-eye anti-reflection structures on graphene sheet based on transformation optics. The reflections of such structures are investigated by analytical Effective Medium Theory combined with Transfer Matrix Method (EMT/TMM) and numerical Finite Element Method (FEM). Both analytical and numerical methods have shown that the average reflection losses of 1% can be achieved within mid-infrared region. Moreover, such performance can be maintained to a very wide incidence angle, achieving less than 1% reflection up to 60° incident angle. The proposed moth-eye anti-reflection structures may provide new visions to achieve biomimetic designs with superior photonic functionalities on graphene-based devices.

OCIS codes: *(240.6680) Surface plasmons;*

References and links

1. S. A. Maier, *Plasmonics: Fundamentals and Applications* (Springer, New York, 2007).
2. K. S. Novoselov, A. K. Geim, S. V. Morozov, D. Jiang, M. I. Katsnelson, I. V. Grigorieva, S. V. Dubonos, and A. A. Firsov, "Two-dimensional gas of massless Dirac fermions in graphene," Nature **438**, 197-200 (2005).
3. L. Ju, B. Geng, J. Horng, C. Girit, M. Martin, Z. Hao, H. A. Bechtel, X. Liang, A. Zettl, Y. R. Shen, and F. Wang, "Graphene plasmonics for tunable terahertz metamaterials," Nature nanotechnology **6**, 630-634 (2011).
4. A. Vakil and N. Engheta, "Transformation optics using graphene," Science **332**, 1291-1294 (2011).
5. R. A. Potyrailo, H. Ghiradella, A. Vertiatchikh, K. Dovidenko, J. R. Cournoyer, and E. Olson, "Morpho butterfly wing scales demonstrate highly selective vapour response," Nature Photonics **1**, 123-128 (2007).
6. T. Khudiyev, T. Dogan, and M. Bayindir, "Biomimicry of multifunctional nanostructures in the neck feathers of mallard (Anas platyrhynchos L.) drakes," Scientific reports **4**, 4718 (2014).
7. M. Kolle, A. Lethbridge, M. Kreysing, J. J. Baumberg, J. Aizenberg, and P. Vukusic, "Bio-inspired band-gap tunable elastic optical multilayer fibers," Advanced materials **25**, 2239-2245 (2013).
8. P. I. Stavroulakis, S. A. Boden, T. Johnson, and D. M. Bagnall, "Suppression of backscattered diffraction from sub-wavelength 'moth-eye' arrays," Optics express **21**, 1-11 (2013).
9. D. G. Stavenga, S. Foletti, G. Palasantzas, and K. Arikawa, "Light on the moth-eye corneal nipple array of butterflies," Proceedings. Biological sciences / The Royal Society **273**, 661-667 (2006).
10. K. Han and C.-H. Chang, "Numerical Modeling of Sub-Wavelength Anti-Reflective Structures for Solar Module Applications," Nanomaterials **4**, 87-128 (2014).
11. W. Gao, J. Shu, C. Qiu, and Q. Xu, "Excitation of plasmonic waves in graphene by guided-mode resonances," ACS nano **6**, 7806-7813 (2012).
12. J. S. Gomez-Diaz and J. Perruisseau-Carrier, "Graphene-based plasmonic switches at near infrared frequencies," Optics express **21**, 15490-15504 (2013).
13. L. A. Falkovsky, "Optical properties of graphene and IV–VI semiconductors," Physics-Uspekhi **51**, 887-897 (2008).
14. J. Tao, X. Yu, B. Hu, A. Dubrovkin, and Q. J. Wang, "Graphene-based tunable plasmonic Bragg reflector with a broad bandwidth," Optics letters **39**, 271-274 (2014).
15. E. E. Perl, W. E. McMahon, R. M. Farrell, S. P. DenBaars, J. S. Speck, and J. E. Bowers, "Surface structured optical coatings with near-perfect broadband and wide-angle antireflective properties," Nano letters **14**, 5960-5964 (2014).

16. E. E. Perl, W. E. McMahon, J. E. Bowers, and D. J. Friedman, "Design of antireflective nanostructures and optical coatings for next-generation multijunction photovoltaic devices," Optics express **22 Suppl 5**, A1243-1256 (2014).
17. E. Hecht and A. Ganesan, *Optics* (Pearson Education, San Francisco, CA, USA, 2002).
18. H. Oraizi and M. Afsahi, "Analysis of planar dielectric multilayers as FSS by transmission line transfer matrix method (TLTMM)," Progress In Electromagnetics Research, PIER (2007).
19. J. Junesch, T. Sannomiya, and A. B. Dahlin, "Optical properties of nanohole arrays in metal-dielectric double films prepared by mask-on-metal colloidal lithography," ACS nano **6**, 10405-10415 (2012).
20. S. J. Wilson and M. C. Hutley, "The Optical Properties of 'Moth Eye' Antireflection Surfaces," Journal of Modern Optics **29**, 993-1009 (1982).

1. Introduction

Surface Plasmons are electromagnetic excitations propagating along the interface between dielectrics and conductors [1]. Graphene is a semiconductor with a two-dimensional form of carbon atoms arranged in the honeycomb lattice [2], leading to the optical properties, such as ultrafast carrier dynamics [10]. Compared with plasmons on the conventional materials, such as noble metals, graphene plasmons (GPs) have shown better characteristics [11] at terahertz frequency band. Moreover, the carrier density in graphene can be electrically tuned by over two orders of magnitude through electrical biasing [3]. Recently, transformation optics (TO) based on graphene have received considerable attentions by offering new possibilities to manipulate the propagation of GPs [4], in which one graphene sheet can be regarded as a compose of spatially inhomogeneous or non-uniform conductivity regions.

The natural world around us provides excellent examples of functional systems built with a handful of materials. Throughout the millennia, nature has evolved to adapt and develop highly sophisticated strategies to generate, detect, absorb, scatter, and otherwise process light. The investigations of such biological systems provide a great number of photonic design opportunities [5-7], e.g. the designs of some highly selective vapor sensors are inspired by the Morpho butterfly wing structures, and the eyes or wings of some species of moth are covered with arrays of nanoscale features that dramatically reduce reflection of light [8]. Multiple examples are proposed where this approach has been adapted for use in antireflection and antiglare technologies with the fabrication of artificial moth-eye surfaces [9, 10].

In this paper we design the biomimetic 'moth-eye' anti-reflection structures on a graphene sheet. In Section 2, the Effective Medium Theory (EMT) combined with Transfer Matrix Method (TMM) have been adopted to describe reflections of such structures and compared with results by numerical methods. In Section 3, we theoretically investigate the wide-angle performances of the proposed anti-reflection structures on the incident wavelength, transition region length and graphene chemical potentials. In the end we draw the conclusion.

2. Theoretical descriptions of moth-eye anti-reflection structures

We first develop in this section an analytical method to describe the anti-reflection functions of the proposed moth-eye anti-reflection structures. The principle by which these anti-reflections structures operate is to create an effective smooth transition across the interface between two mediums, and therefore ensures that incident light would not encounter a sudden change in refractive index, which would generally lead to the reflection of a proportion of energy [8]. Such biomimetic structures could provide superior anti-reflection performances within broad frequency band and under wide incident angles. On the other hand, according to the transformation optics [4], when the graphene plasmons (GPs) encounter two regions with different conductivities (Fig. 1(a)), the situation can be treated as an analogy of the plane wave passing from one medium to another (upper panel of Fig.1(b)). The modal indexs of GPs on the two regions $Neff_1$ and $Neff_2$ can be regarded as the medium refractive indexs. The smooth transition in refractive indexs provided by biomimetic anti-reflection structures can be obtained from the Effective Medium Theory (EMT) (lower panel of Fig.1 (b)). The length of anti-reflection structures is L_2.

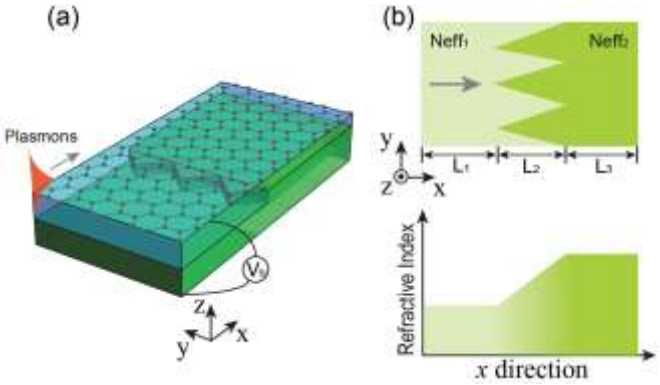

Fig. 1. Schematic view of the graphene sheet waveguide (a) and the equivalent structure based on transformation optics (upper panel of (b)) and the refractive index variation from effective medium theory.

The realistic situation is illustrated in Fig. 1(a), a pattern-free graphene sheet is placed on an uneven doped silicon substrate with a dielectric spacer between them. Since the spacer has distinct thicknesses for the two regions, with a biased voltage V_b applied between graphene and doped silicon substrate, the difference of spacer thicknesses naturally lead to the different graphene chemical potentials on those two regions [11, 12]. In the mid-infrared frequency, the conductivity of graphene can be modeled with a semi-classical Drude model with a finite temperature correction as [13],

$$\sigma(\omega) = \frac{2e^2}{\pi\hbar} K_{\cdot\cdot} T \times \ln\left[2\times\cosh(\frac{\mu_c}{2K_B T})\right]\frac{j}{\omega + j\tau^{-1}} \qquad (1)$$

where j is the imaginary unit, e is the unit electric charge, $\hbar$ is the reduced Planck constant, K_B is the Boltzmann constant, μ_c is the graphene chemical potential, T=300 K is the temperature and ω is the angular frequency. The carrier relaxation time τ can be determined through $\tau = u\mu_c/ev_f^2$, where the carrier mobility u =10^4 cm^2/(V·s) and the Fermi velocity v_f =10^6 m/s [11]. The surface-normal permittivity of graphene is assumed as $\varepsilon_{g,n}$=2.5, based on the dielectric constant of graphite [13, 14]. By treating the graphene as an ultrathin layer with thickness d=0.34 nm, the tangential permittivity of graphene can be expressed as $\varepsilon_{g,t}$=2.5-i$\sigma/\omega\varepsilon_0 d$ [11]. The maximum chemical potential of graphene is set as μ_c=0.7 eV, which can be implemented through electronic biasing [11, 12]. The dispersion relation of graphene plasmons can be approximately expressed as $\beta \approx j\omega\varepsilon_0(\varepsilon_1+\varepsilon_2)/\sigma(\omega)$ or the following form if Eq. (1) is substituted,

$$\beta \approx \frac{\pi\hbar^{\hat{}}}{e^2\mu_c}(\varepsilon_1+\varepsilon_2)(1+\frac{j}{\omega\tau})\omega^2 \qquad (2)$$

where ε_1=1 and ε_2=1.76 are the dielectric constants of the mediums above and the dielectric spacer without dispersion and dielectric loss. All the numerical solutions have been performed by the software package (COMSOL) based on Finite Element Method (FEM). According to the Eq. (2), the modal indexs of GPs as functions of chemical potentials and wavelengths can be derived. The real and imaginary parts of indexs are respectively shown in Fig. 2(a) and 2(b). The wavelength spans from 6 μm to 10 μm while chemical potential varies from 0.2 eV to 0.7 eV. As rendered in Fig. 2(a), higher wavelength or chemical potential leads to the lower modal index and vice versa. Moreover, unlike the real part, the imaginary part in Fig. 2(b) performs much weaker dependence on wavelength while can still be adjusted by chemical potential. Higher real index means strong field confinement and simultaneously leads to the larger attenuation. It should be noted that for one wavelength (e.g. 6μm), the real index gap under different chemical potentials can be nearly 50. Once GPs propagate between regions

with large chemical potential gap (e.g. from 0.7 eV to 0.2 eV), considerable reflection is unavoidable.

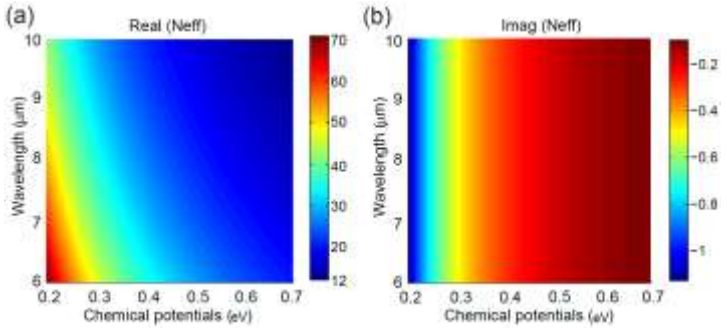

Fig. 2. Dependencies of the real and imaginary graphene plasmons modal indexs N_{eff} on the wavelengths and chemical potentials..

To describe the anti-reflection functions of such structures, one may slice the middle region with smooth transitional refractive indexs into a large number of thin layers along x direction [15, 16]. Each layer is with thickness L_2/N and the according effective index can be derived from EMT (see Fig. 1(b)), where N=100 to ensure the spacing between adjacent slices is less than the shortest plasmons wavelength considered. Afterwards, the reflectance off and transmittance through can be obtained by Transfer Matrix Method (TMM). The TMM is a simple approach to model waves passing through multilayer layers [10]. It employs continuity boundary conditions between dielectric layers and wave equations to describe reflection or transmission across each layer. Then, if the electric field is known at the beginning of the layer, a transfer matrix based on the wave equation can be used to determine the electric field at the other end of the layer [17, 18]. Compared with other methods adopted in analyzing multilayer structures, such as the Time-Based Optical Modeling Methods (e.g. FDTD), Rigorous Coupled Wave Analysis (RCWA) or the FEM, the TMM owes the fastest computation speed with satisfactory accuracy [10]. More detailed information about the TMM we adopted in this paper can be found in the supporting information of [19].

We next present the reflection spectrums of the proposed structure by both analytical and numerical methods with alternative middle region lengths L_2 and chemical potentials (under single biased voltage). For simplicity, the lengths of the first and last region are fixed at L_1 =L_3=100 nm with the plasmons attenuations on which have been taken into account. The chemical potentials of the two regions are respectively μ_{c1}=0.7eV and μ_{c2}=0.4 eV in Fig. 3(a) and the middle region length L_2=100 nm in Fig. 3(b). The wavelength spans from λ= 6 μm to 10 μm.

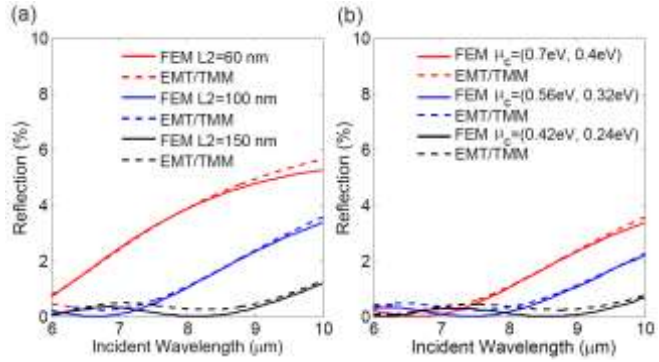

Fig. 3. Dependencies of the reflection spectrum under distinct middle region length L_2 (a) and chemical potentials of two regions (b).

As rendered in Fig. 3(a), the reflectance decreases at larger length L_2. The reflectance within the whole considered wavelengths can be under 1% at L_2=150 nm. It can be explained by considering the length L_2 approaching the order of half a graphene plasmons wavelength (can be calculated from Fig. 2(a)), therefore the reflectance can be considerably reduced [20]. Figure 3(b) shows that the reflectance can be tuned by the chemical potentials through biased voltage. The reason is similar to that in Fig. 3(a), the chemical potential influences the real modal index, which further affects the graphene plasmons wavelength. Lower potential gives rise to the higher modal index and lower plasmons wavelength afterwards, making plasmons wavelength and length L_2 comparable and reducing reflectance. Furthermore, the analytical results from EMT/TMM agree very well with numerical method (error<0.5%), implying that the EMT/TMM can be adopted in the design of such anti-reflection structures.

3. Anti-reflection performances under wide incident angle

In this section, we investigate the wide-angle anti-reflection performances of the biomimetic 'moth-eye' structures on graphene sheet by the EMT/TMM. In the practical applications, although the numerical simulations could provide rigorous solutions, they are quite time- and resource-consuming. As mentioned before, the EMT/TMM provides the fastest calculation speed, physical insight as well as satisfactory consistency to rigorous numerical simulations. Thus we suggest the analytical methods can be the 'first step' in the design procedure and numerical simulations afterwards. Firstly, we present the reflection spectrums under various incident angles and wavelengths in Fig. 4(a) and middle region length L_2 in Fig. 4(b) through analytical methods. The chemical potentials are set as μ_{c1}=0.7 eV and μ_{c2}=0.4 eV.

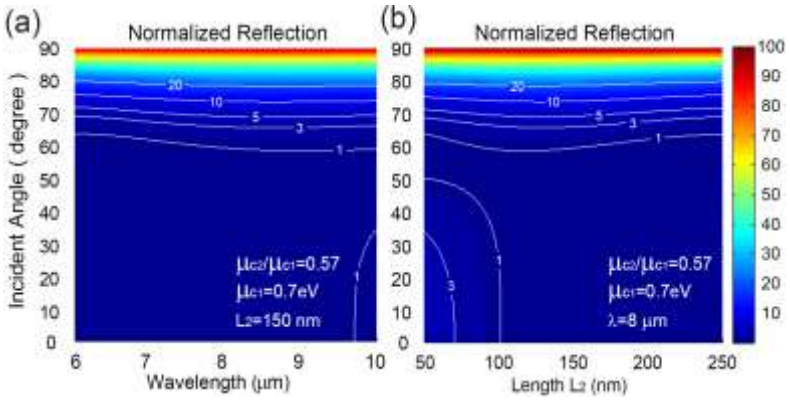

Fig. 4. Dependencies of normalized reflections by EMT/TMM on the incident wavelength (a) and middle region length L_2 (b). The parameters settings are shown in the figure.

As shown in the Fig. 4(a), the proposed 'moth-eye' anti-reflection structures possess well wide-angle performances, achieving reflections below or around 1% up to 60° incident angle and below 20% up to 80° incident angle. Moreover, as shown in Fig. 4(b), larger length L_2 should be chosen for small angle incidence (<50°). While for the larger incident angle (between 50° and 60°), the reflection shows unobvious dependence on the length L_2. Such biomimetic anti-reflection structures can be applied as boundary to prevent the scatterings of incident GPs in the graphene-based devices. Secondly, as shown in Fig. 3(b), the reflection can be tuned by chemical potential on the two regions. Therefore, we assume two situations and investigate the wide-angle anti-reflection performances. One is the two regions under same varied biased voltage with fixed spacer thicknesses, resulting in the fixed chemical potentials ratio μ_{c2}/μ_{c1}. While in the other case, the two regions owe varied dielectric spacer thicknesses with same biased voltage, giving rise to the different chemical potential ratios. For simplicity, we set μ_{c1} as the independent variable and μ_{c2} as the dependent variable. In Fig. 5(a), the ratio is fixed while μ_{c1} spans from 0.3 eV to 0.7 eV. While in Fig. (b), the μ_{c1} is fixed

at 0.7 eV and chemical ratio spans from 0.1 to 0.9. The settings of wavelength and middle region length L_2 are shown in the figures.

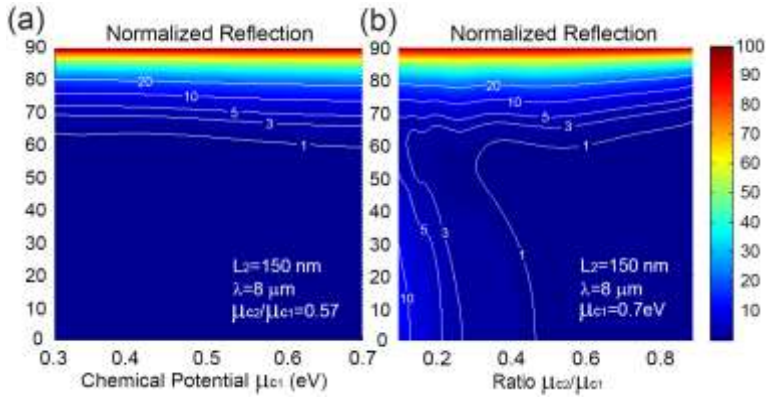

Fig. 5. Dependencies of normalized reflections by EMT/TMM on the chemical potential μ_{c1} under same biased voltage (a) and the chemical potentials ratio with μ_{c1} is fixed. The parameters settings are shown in the figure.

Figure 5(a) renders that the reflections are nearly independent on the biased voltage under sufficient long transition region (L_2=150 nm), which means that the proposed structure can still perform well even at quite smaller biased voltages, cutting implement complexities and becoming more easily realized. On the other hand, in Fig. 5(b) the reflections show obvious dependences on the chemical potential ratios. The lower ratio means the larger index gap between the two regions and accordingly high reflection, therefore suitable L_2 (near the order of half a graphene plasmons wavelength) is needed to achieve low reflection.

Conclusion

In this paper, we proposed a biomimetic 'moth-eye' anti-reflection structures on the graphene sheet. As the graphene plasmons propagate on the graphene sheet with two spatially distinct chemical potentials, the reflectance can be reduced by introducing one layer with smooth transition of plasmons modal index. The reflectance derived from Effective Medium Theory (EMT) and Transfer Matrix Method (TMM) shows well consistency to the numerical methods. Reflectance below 1% can be achieved in the mid-infrared frequency band with well wide-angle performances. Theoretical investigations show that for the structures with enough length, the reflectance is nearly independent on the biased voltage, while for the case with large chemical potential gap, the length should be appropriately selected. The proposed structures pave ways to achieve analogies of biological structures with superior photonic functionalities on the graphene-based devices.

Acknowledgment

This work is supported in part by the National Natural Science Foundation of China (NSFC) (Grant Nos. 61178008, 61275092).